AIP Advances

RESEARCH ARTICLE | MARCH 14 2025

Pressure effect on electronic and optical properties of noncentrosymmetric $LaPtGe_3$ studied by *ab initio* method

Md. Karimul Islam; Nilufer Yesmin Tanisa ; Mosfiqur Rahman; Abul Monsur Musa; Tareque Aziz ; Md. Moiful Alam ; Asif Pervez

Check for updates

AIP Advances 15, 035327 (2025)
https://doi.org/10.1063/5.0255737

View Online
Export Citation

Articles You May Be Interested In

High-throughput structural screening and property study of noncentrosymmetric superconductors in Th-based ZrNiAl-like compounds

J. Appl. Phys. (November 2024)

Exploration of noncentrosymmetric superconductors in the ZrNiAl family via high-throughput *ab-initio* calculations

J. Appl. Phys. (June 2025)

Superconductivity in Noncentrosymmetric BiPd System

AIP Conf. Proc. (July 2011)

25 March 2026 03:03:50

AIP Publishing

Special Topics Open for Submissions

Learn More

AIP Publishing

Pressure effect on electronic and optical properties of noncentrosymmetric $LaPtGe_3$ studied by *ab initio* method

Cite as: AIP Advances 15, 035327 (2025); doi: 10.1063/5.0255737
Submitted: 31 December 2024 • Accepted: 16 February 2025 •
Published Online: 14 March 2025

View Online Export Citation CrossMark

Md. Karimul Islam, Nilufer Yesmin Tanisa,[a] Mosfiqur Rahman, Abul Monsur Musa, Tareque Aziz, Md. Moiful Alam, and Asif Pervez

AFFILIATIONS

Department of Physics, Uttara University, Dhaka 1230, Bangladesh

[a]Author to whom correspondence should be addressed: tanisha.90@uttarauniversity.edu.bd

ABSTRACT

Density functional theory applied with the CASTEP algorithm was used to evaluate the electrical and optical characteristics of $LaPtGe_3$. The band structure reveals overlapping bands at the Fermi level, indicative of metallic behavior, with Ge-4p states playing a dominant role in electrical conductivity. Pressure-induced changes in the density of states and Ge–Ge bond lengths suggest a significant influence on the optical and thermodynamic properties of $LaPtGe_3$. Reflectivity increases under external pressure, exhibiting anisotropic behavior along the crystallographic axes, particularly around 17 eV along the [001] direction. Absorption spectra show a metallic response starting from zero photon energy, with maximum absorption near 20.50 eV and transparency beyond 50 eV. Increased pressure enhances absorption, making the material more viable for solar cell applications under high pressure. Photoconductivity also begins at zero photon energy, confirming the absence of a bandgap. The anisotropic nature is evident in absorption and conductivity spectra across all pressure ranges. The bulk plasma frequency, measured at 25.65 eV, increases with pressure, while the refractive index shows a high initial value followed by a decline in the infrared, visible, and ultraviolet regions. The components of the dielectric function's real (ε_1) and imaginary (ε_2) confirm metallic characteristics. These findings highlight the potential of $LaPtGe_3$ for applications in optoelectronics and high-pressure environments.

© 2025 Author(s). All article content, except where otherwise noted, is licensed under a Creative Commons Attribution (CC BY) license (https://creativecommons.org/licenses/by/4.0/). https://doi.org/10.1063/5.0255737

25 March 2026 03:03:50

I. INTRODUCTION

The layered ternary intermetallic compounds with transition metal components of the $BaNiSn_3$ type have been extensively explored for their rich and attractive physical features.[1] The ternary intermetallic combination $LaPtGe_3$ belongs to group 14(IVA) of the periodic table,[2] where La is usually a silvery alkaline earth metal, Pt is a silverfish-white transition metal, and Ge is an element, forming the largest family member by crystallizing in the $BaNiSn_3$ type body-centered tetragonal structure (space group I4mm) (No. 107). This chemical has recently garnered significant attention from academics due to its diverse physical characteristics. The ternary of $BaNiSn_3$ type also exhibits the last events on superconductivity. The parent barium-pnictide superconductor compounds $LaMGe_3$ (M = Pd, Pt, Rh, Ir, etc.) with a similar $BaNiSn_3$-type crystal structure have been the subject of much investigation due to their distinct physical characteristics.[3] Ternary intermetallic compounds with $BaAl_4$-type structures are thought to be among the most significant intermetallic families.[4] BaNiSn: three types of family members have received a lot of attention[5–8] because many of them have unusual properties and a variety of low-temperature physical properties, such as complex magnetic ordering,[9,10] valence fluctuation,[11] the Kondo effect,[12] and phase transition.[13,14] We provide measurements of the temperature dependence of magnetic penetration depth in a high-quality sample of $LaPtGe_3$. We detect a temperature-independent nature below T = 0.2 Tc, which provides strong evidence for the occurrence of an isotropic superconducting gap in this material. A strong-coupling the Bardeen–Cooper–Schrieffer (BCS) model with an isotropic gap $\Delta_0 = 2k_BTc$ effectively describes the superfluid density over the temperature range. Our findings lend credence

© Author(s) 2025

to conventional BCS superconductivity in nonmagnetic members of the non-centrosymmetric superconductor family that crystallize with the $BaNiSn_3$-type tetragonal structure.[15] These compounds exhibit extremely appealing and rich physics because of their near energies in terms of spin, charge, and orbital dynamics.[16] $LaPtGe_3$ is a type-I superconductor with s-wave pairing, while $CePtGe_3$ is a nonsuperconducting metal exhibiting antiferromagnetic ordering due to magnetic interactions. The compounds exhibit contrasting behaviors, with $LaPtGe_3$ displaying superconductivity and $CePtGe_3$ forming a magnetically ordered ground state.[17] The LaNiSi, LaPtSi, and LaPtGe 111-family materials exhibited Weyl nodal-line fermions and transitioned into a fully gapped superconducting state that breaks time-reversal symmetry. This behavior indicates a topological phase transition, providing an ideal system to study the interaction between Weyl nodal-line fermions and unconventional superconductivity.[18] $EuPtGe_3$, with a non-centrosymmetric structure, exhibits a magnetic transition, characterized by susceptibility, heat capacity, and Mössbauer spectroscopy, indicating a slight first-order nature. Its magnetic behavior is explained using a mean-field model with antiferromagnetic sublattices, revealing key exchange interactions.[19] The spin–orbit coupling's effects on LaPtGe and $LaPtGe_3$ revealed s-wave superconductivity driven by electron–phonon interactions, with medium coupling in LaPtGe and weak coupling in $LaPtGe_3$.[20] Spin–orbit coupling slightly impacts LaPtGe more due to its d-shell-dominated electronic structure near the Fermi level. In this article, we conducted a detailed theoretical examination of the layered ternary $LaPtGe_3$ utilizing a first-principles technique based on density functional theory (DFT) and the CASTEP code. The current work aims to examine the electrical and optical characteristics of $LaPtGe_3$. The primary goal of this investigation is to find the equilibrium structure. The spatial arrangement of atoms in a material influences numerous aspects, including its electrical band structure and optical qualities. The electronic band structures, as well as the total and partial density of states (DOS), have been estimated for various pressures. The optical characteristics of the dielectric function, refractive index, reflectivity, absorption coefficient, energy loss function, and conductivity as a function of photon energy along the [100], [010], and [001] directions have been investigated.

The noncentrosymmetric $LaPtGe_3$ compound has a tetragonal crystal structure with the space group I4mm (No. 107).[1] The Wyckoff coordinates for this compound are 2a (0, 0, 0.0001) for La, 2a (0, 0, 0.3474) for Pt, 2a (0, 0, 0.5971) for Ge 1, and 4b (0, 1/2, 0.2401) for Ge 2.[17] In this study, calculations were performed using an *ab initio* plane wave pseudopotential (PWPP) method in the framework of density functional theory (DFT) using generalized gradient approximation (GGA) with the implementation of CASTEP code to investigate structural, electronic, and optical properties.

II. CALCULATION SCHEMES

A. Computation of different properties of $LaPtGe_3$

All computations were performed with the Cambridge Serial Total Energy Package (CASTEP) tool, which is based on density functional theory (DFT).[21] The exchange-correlation energy function was defined using Perdew–Burke–Ernzerhof's generalized gradient approximation (GGA).[22] Coulomb interactions between valence electrons and the ionic core were described using Vanderbilt-type ultrasoft pseudopotentials.[23] The cutoff energy value for the plane-wave basis set was chosen as 350.0 eV for $LaPtGe_3$. Monkhorst–Pack techniques[24] were used to estimate the energy in the irreducible Brillouin zone with 12 × 12 × 6 grids of k-points. The structural optimizations were performed using Broyden–Fletcher–Goldfarb–Shanno (BFGS) minimizations.[25] To optimize geometry, the convergence tolerance was set as follows: the total energy convergence value is within 5.0×10^{-6} eV/atom, the maximum Hellmann–Feynman force is within 0.01 eV/Å, the maximum displacement is within 0.005 Å, the maximum stress is within 0.02 GPa, and the maximum iterations were set to 100. $LaPtGe_3$'s elastic constants are found using the stress–strain technique.[20] The maximum strain amplitude was set to 0.003. The elastic constants were calculated using convergence tolerance requirements of 1.0×10^{-6} eV/atom for total energy, 0.002 eV/Å for maximum force, and 1.0 × 10−4 Å for maximum displacement.

B. Geometry optimization

Geometry optimization is used to identify minima on the potential energy surface, which indicate equilibrium structures. Optimization is used to identify transition structures, which are represented by saddle points on the potential energy surface.

C. Electronic properties

One of the most beneficial features of the band structure is the bandgap, which has a significant impact on the material's electrical and optical characteristics as well as a compound's stability in the face of oxidation or reduction (doping). Through the processes of carrier creation and recombination, electrons can move between bands. Solar cells, diodes, transistors, laser diodes, and other semiconductor devices may be made using the bandgap and defect states that doping creates in the bandgap. Moreover, the crystal structure and the energy levels of the component atomic orbitals determine the band structure. In the Brillouin zone (BZ), each state is identified by its wavenumber (k). For a big crystal, this wave number is packed very tightly within the Brillouin zone. The first band is the lowest lying state of a certain wavenumber; the second band and soon are the following lying states of the same wavenumber. Therefore, the wavenumber and band index of each electrical state are provided. Every condition, of course, has a distinct energy. As in the case of one dimension, the energy of the n-th band will thus be represented by $E_n(k)$, which turns out to be a quasi-continuous function of wavenumber for each band. When the wavenumbers permitted by the periodic boundary conditions are fairly close together, the function for a big crystal becomes very nearly continuous.

D. Density of states (DOS)

Many states are accessible for occupancy when the DOS is high for a given energy level. No states can be occupied at that energy level if the DOS is zero. A DOS is often an average over the system's time and space domains. The local density of states (LDOS) is a term used to describe local variances, which are often caused by distortions of the original system. Because of the existence of a local

25 March 2026 03:03:50

© Author(s) 2025

potential, the LDOS of an undisturbed system may be locally non-zero even if the DOS is zero.[26] The number of states in the system where the energy under consideration is multiplied by the probability distribution function must be known to calculate the actual number of electrons in a given energy level. The number of available quantum states in the energy range ε to $\varepsilon + d\varepsilon$ is $g(\varepsilon)d\varepsilon$, and $F(\varepsilon)$ represents the probability of occupation. Therefore, the actual number of electrons in this energy range at any temperature is

$$dN = g(\varepsilon)F(\varepsilon)d\varepsilon. \tag{2.1}$$

The quantity $g(\varepsilon)$, known as the density of states (DOS), differs between classical and quantum values. Generally, the DOS represents the spectrum of energy levels per eV as a function of energy. It serves as a qualitative tool for understanding the electronic structure of materials. In addition, the partial density of states (PDOS) is valuable, as it attributes states to the basis functions and atoms within the unit cell. The total DOS is then obtained by summing the atomic contributions. The DOS is calculated using the following expression:

$$n(\varepsilon) = 2\sum_{n,\mathrm{k}} \delta\left(\varepsilon - \varepsilon_n^k\right) = \frac{2}{V_{BZ}}\sum_n \int \delta\left(\varepsilon - \varepsilon_n^k\right) d\,\mathrm{k}, \tag{2.2}$$

where δ denotes the Dirac delta function, and the integral over k extends across the BZ.

The number of electrons in the unit cell is given by $\int_{-\infty}^{\varepsilon_F} n(\varepsilon)d\varepsilon$.

E. Optical properties

Calculating optical spectra involves considering both the occupied and unoccupied states of the electronic structure, as well as the characteristics of the bands. The dielectric function, $\varepsilon(\omega) = \varepsilon_1(\omega) + \varepsilon_2(\omega)$, describes the optical response of a medium at all photon energies $\hbar\omega$. The imaginary part of the dielectric function, $\varepsilon_2(\omega)$, is determined by summing transitions from occupied to unoccupied states. Specifically, in this study, $\varepsilon_2(\omega)$ is expressed as follows:

$$\varepsilon_2(\omega) = \frac{2e^2\pi}{\Omega\varepsilon_0}\sum_{k,v,c} \left|\psi_k^c\middle|u\cdot r\middle|\psi_k^v\right|^2 \delta\left(E_k^c - E_k^v - \hbar\omega\right), \tag{2.3}$$

where $\boldsymbol{u}$ represents a vector defining the polarization of the incident electric field, $\boldsymbol{e}$ is the electronic charge, and ω denotes the light frequency. The wave functions ψ_k^v and ψ_k^c correspond to the valence and conduction bands at wave vector $\mathbf{k}$, respectively. The Kramers–Kronig relation allows the real part of the dielectric function to be derived from the imaginary part, as expressed in the form.[12,13] The equation is given as

$$\varepsilon_1(\omega) = 1 + \frac{2}{\pi}P\int_0^\infty \frac{\omega'\varepsilon_2(\omega')}{\omega'^2 - \omega^2}d\omega', \tag{2.4}$$

where P implies the principal value of the integral.

Having both the real and imaginary components of the dielectric tensor provides the necessary information to compute key optical functions. In this work, we examined and discussed several properties, including the reflectivity $R(\omega)$, absorption coefficient $I(\omega)$, optical conductivity $\sigma(\omega)$, electron energy loss spectrum $L(\omega)$, refractive index $n(\omega)$, and extinction coefficient $k(\omega)$. The reflectivity spectra are obtained using Fresnel's formula for normal incidence, assuming the crystal surface is oriented parallel to the optical axis, as expressed in the relation[16]

$$R(\omega) = \left|\frac{\sqrt{\varepsilon(\omega)} - 1}{\sqrt{\varepsilon(\omega)} + 1}\right|^2. \tag{2.5}$$

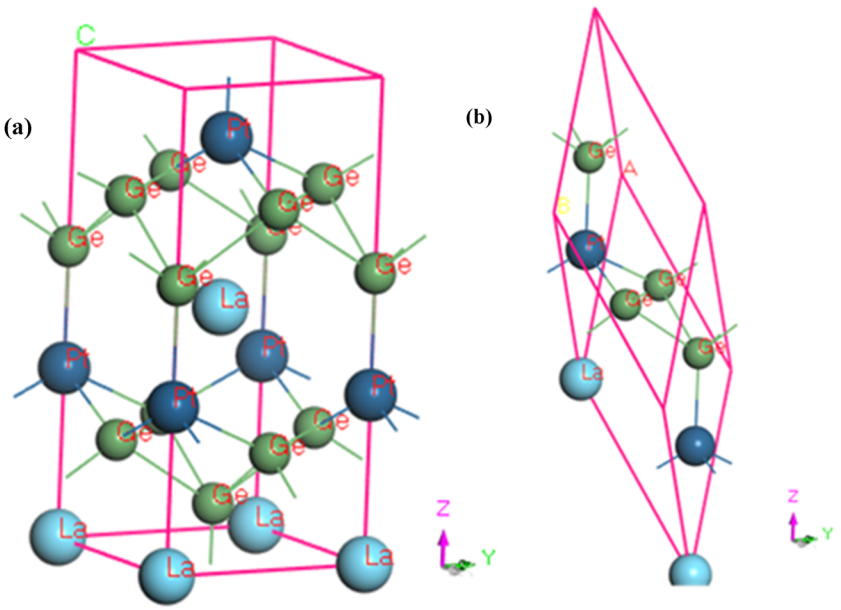

FIG. 1. Crystal structure of $LaPtGe_3$: (a) Conventional unit cell and (b) primitive unit cell.

25 March 2026 03:03:50

© Author(s) 2025

TABLE I. Optimized unit cell parameters ($a = b$ and c Å) and unit cell volume of the $LaPtGe_3$ compound under different pressures.

Pressure (GPa)	$a = b$ (Å)	C (Å)	V_0 (Å^3)	c/a	Energy, E (eV)
0	4.523 336	9.916 621	202.89	2.192 32	−3806.69
5	4.459 753	9.771 288	194.34	2.190 99	−3806.56
10	4.406 281	9.656 279	187.48	2.191 48	−3806.24
15	4.356 154	9.579 505	181.78	2.199 07	−3805.79
20	4.316 648	9.489 520	176.82	2.198 35	−3805.25
25	4.279 208	9.419 833	172.49	2.201 30	−3804.65

The optical properties, including reflectivity $R(\omega)$, absorption coefficient $I(\omega)$, refractive index $n(\omega)$, and energy-loss spectrum $L(\omega)$, can all be derived from $\varepsilon_1(\omega)$ and $\varepsilon_2(\omega)$,[27,28]

$$I(\omega) = \sqrt{2}(\omega)\left(\sqrt{\varepsilon_1(\omega)^2 + \varepsilon_2(\omega)^2} - \varepsilon_1(\omega)\right)^{1/2}, \quad (2.6)$$

$$n(\omega) = \left[\frac{\varepsilon_1(\omega)}{2} + \frac{\sqrt{\varepsilon_1(\omega)^2 + \varepsilon_2(\omega)^2}}{2}\right]^{1/2}, \quad (2.7)$$

$$L(\omega) = \frac{\varepsilon_2(\omega)}{\varepsilon_1(\omega)^2 + \varepsilon_2(\omega)^2}. \quad (2.8)$$

The extinction coefficient $k(\omega)$ and other optical spectra can be easily computed using the components of the complex dielectric function, as shown below:

$$k(\omega) = \left[\frac{\sqrt{\varepsilon_1(\omega)^2 + \varepsilon_2(\omega)^2}}{2} - \frac{\varepsilon_1(\omega)}{2}\right]^{1/2}. \quad (2.9)$$

TABLE II. Experimental lattice parameters and unit cell volume of $LaPtGe_3$.

Properties	Experimental values
$a = b$ (Å)	4.5064
c (Å)	9.8239
c/a	2.18
V_0 (Å^3)	199.50

III. RESULTS AND DISCUSSION

A. Crystal structure of $LaPtGe_3$

Figure 1 shows the conventional primitive unit cell of the $LaPtGe_3$ compound. The lattice parameters of the optimized $LaPtGe_3$ have been tabulated in Table I. The equilibrium crystal structure of this compound is optimized by minimizing its total energy. Figure 2 shows the total energy vs (a) cutoff energy and (b) k-points of the $LaPtGe_3$ compound.

A 12 × 12 × 6 Monkhorst grid was employed to adequately sample the Brillouin zone [Fig. 1(b)]. The structure was fully optimized until the internal stress and forces on each atom became negligible. For all relevant calculations, a plane wave basis set cutoff of 350 eV was used, as depicted in Fig. 1(a). The experimental lattice parameters are listed in Table II. The optimized equilibrium lattice parameters align with other available experimental values. However, slight deviations from the experimental parameters were observed due to the temperature dependence of the cell parameters and the GGA process.[29] It is observed that both the lattice parameters and unit cell volume gradually decrease with increasing pressure.

B. Electronic properties

The electronic properties of $LaPtGe_3$ have been studied through an analysis of the electronic band structure, partial density of states (PDOS), and total density of states (TDOS). The band structures, examined along the high-symmetry directions within the Brillouin zone (BZ), are illustrated in Fig. 3. The Fermi level is indicated by the dotted line. Energy bands situated below the Fermi level correspond

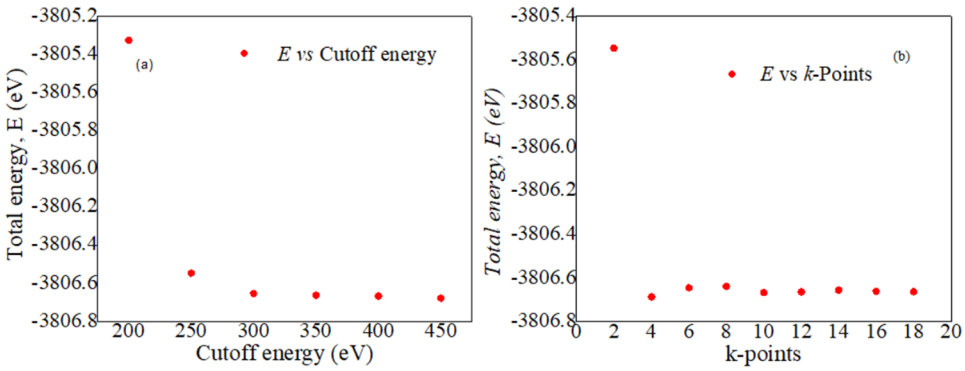

FIG. 2. Total energy vs (a) cutoff energy and (b) k-points of the $LaPtGe_3$ compound.

25 March 2026 03:03:50

© Author(s) 2025

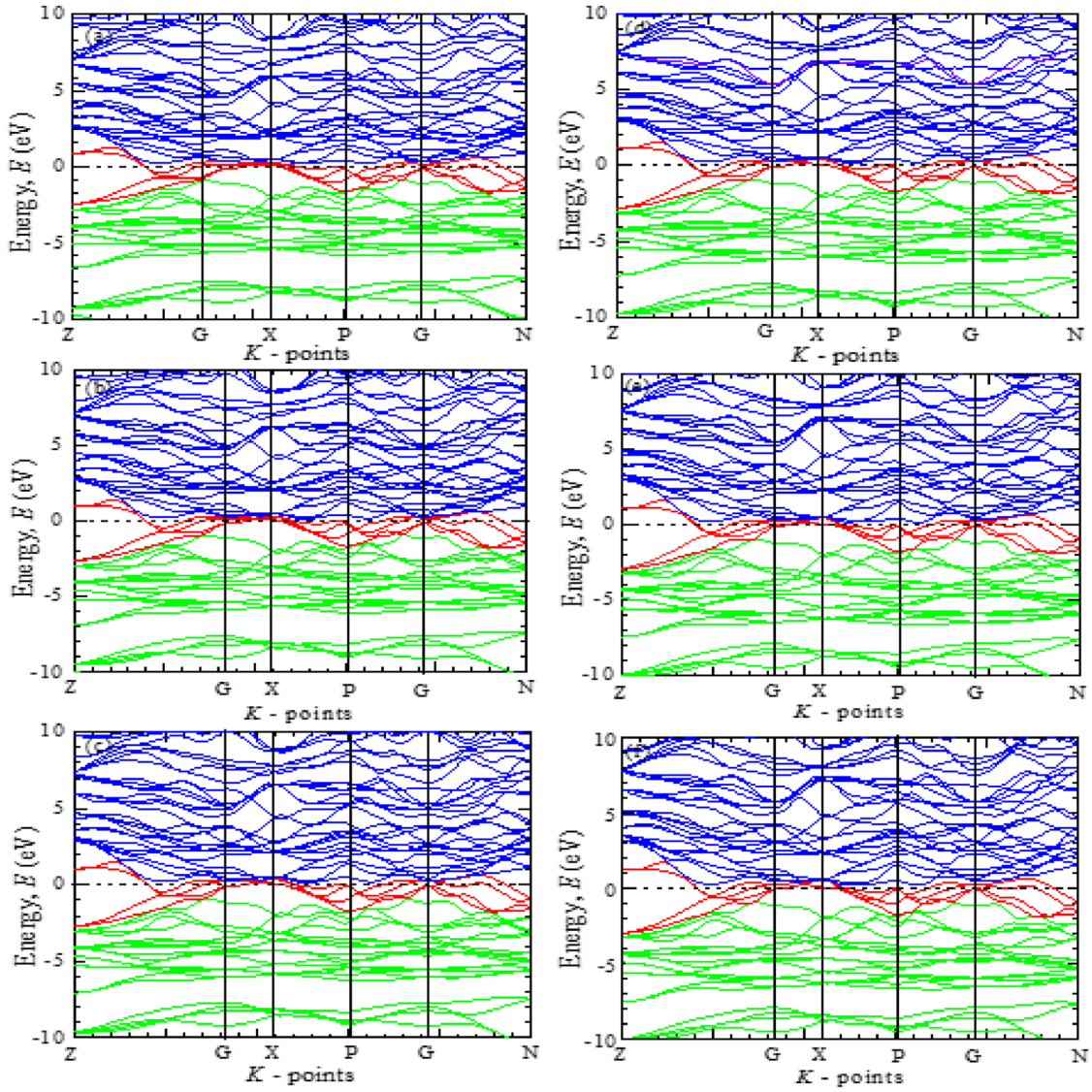

FIG. 3. Electronic band structures of $LaPtGe_3$ at (a) $P = 0$ GPa, (b) $P = 5$ GPa, (c) $P = 10$ GPa, (d) $P = 15$ GPa, (e) $P = 20$ GPa, and (f) $P = 25$ GPa along the high-symmetry directions in the irreducible Brillouin zone.

to the valence bands, while those above represent the conduction bands. Figure 3 reveals that some bands overlap with the Fermi level, which spans approximately from −3 to 1 eV, indicating the metallic nature of the $LaPtGe_3$ material. To gain further insight into the electronic structure of $LaPtGe_3$, both the total density of states (TDOS) and partial density of states (PDOS) have been analyzed. The calculated TDOS and PDOS for $LaPtGe_3$ under ambient conditions and external pressures of 5, 10, 15, 20, and 25 GPa are presented in Figs. 4–6.

At ambient pressure, the total density of states (DOS) of $LaPtGe_3$ at the Fermi level (EF) is 2.554 electrons/eV, with contributions from various states, including Pt-6*s*, Pt-5*p*, Pt-5*d*, La-6*s*, La-5*p*, La-5*d*, Ge-4*s*, and Ge-4*p*. Figures 4–6 show that the primary contribution to the total DOS at the Fermi level comes from the Ge-4*p* states. This suggests that $LaPtGe_3$ displays metallic behavior, primarily due to the dominance of Ge-4*p* states at the Fermi level. The total and partial DOS of $LaPtGe_3$ under varying pressures are summarized in Table III. It is noted that the total DOS at the Fermi level increases slightly with increasing external pressure (0–20 GPa) before decreasing. This trend suggests that the metallic nature and electrical conductivity of $LaPtGe_3$ are enhanced under pressure, likely due to the reduction in the Ge–Ge bond length. Changes in

25 March 2026 03:03:50

© Author(s) 2025

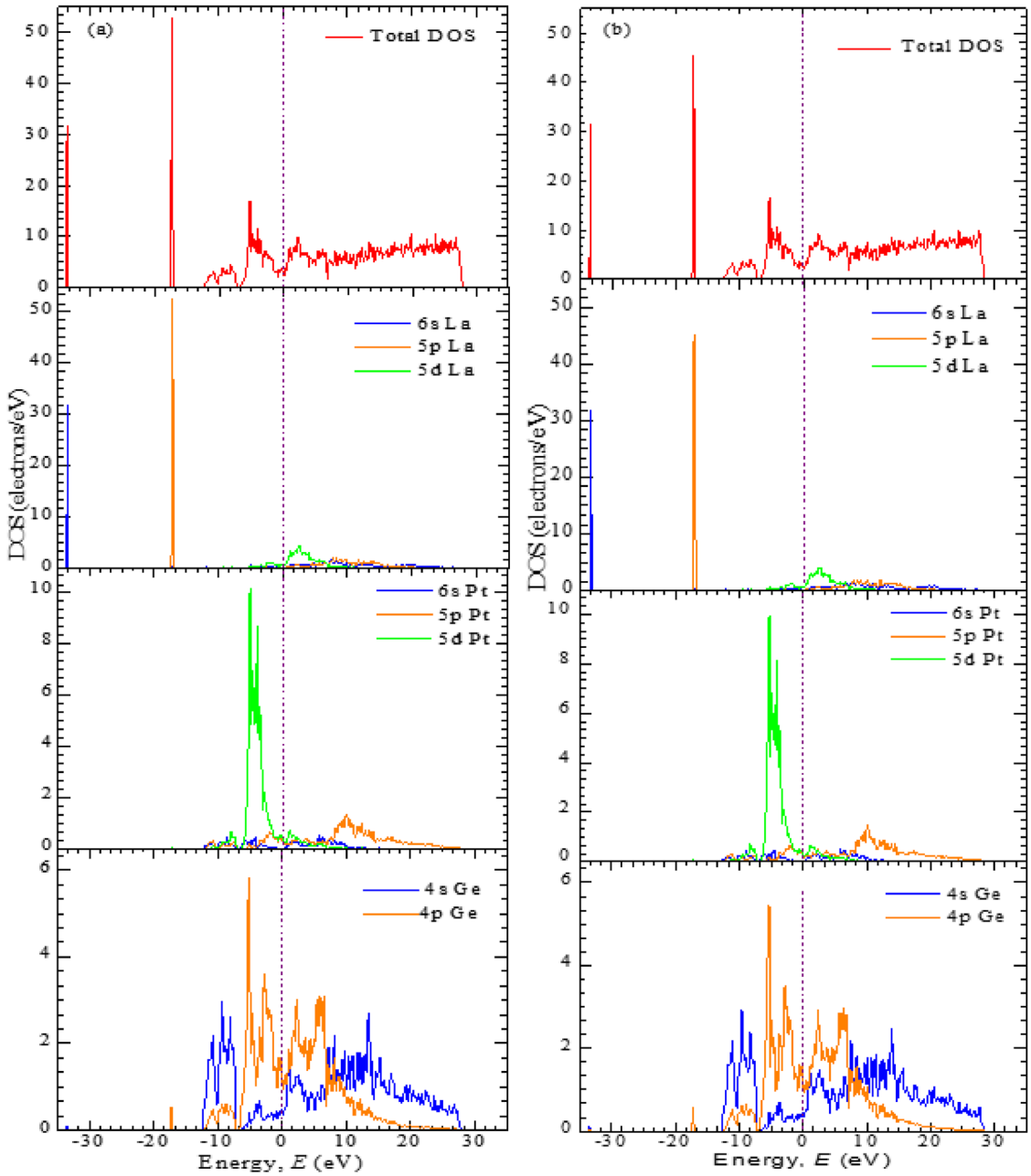

FIG. 4. Total and partial density of states (DOS) of $LaPtGe_3$ at (a) $P = 0$ GPa and (b) $P = 5$ GPa.

the DOS and Ge–Ge bond lengths may also impact other properties of $LaPtGe_3$, such as its optical and thermodynamic characteristics.

C. Optical properties

This section examines various optical constants, including absorption, conductivity, dielectric functions, loss function, reflectivity, and refractive index. These properties are crucial for understanding the material's interaction with light and its overall optical behavior. Absorption indicates how much light is absorbed by the material, while conductivity relates to its ability to conduct electricity under an external electric field. The dielectric function describes the material's response to an applied electric field, affecting its polarization and propagation of electromagnetic waves.

25 March 2026 03:03:50

© Author(s) 2025

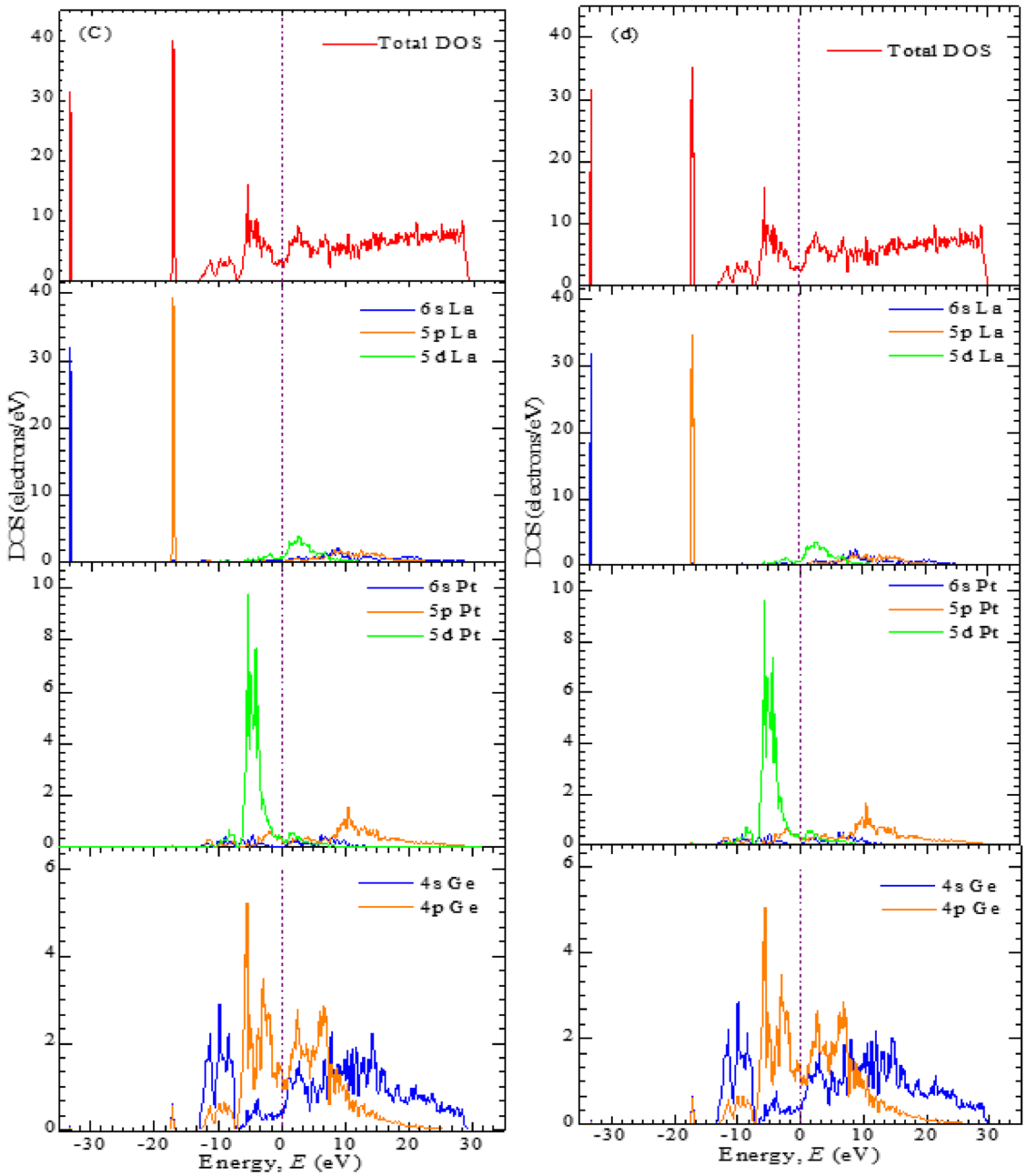

FIG. 5. Total and partial density of states (DOS) of $LaPtGe_3$ at (c) P = 10 GPa and (d) P = 15 GPa.

The loss function characterizes energy dissipation within the material, and reflectivity measures the amount of light reflected off its surface. Eventually, the refractive index provides insight into how light travels through the material, influencing its bending and transmission.

Reflectivity is an optical characteristic of a material that indicates the proportion of light reflected from it compared to the amount of light incident on the material. This property is influenced by several factors, including the wavelength of light, the angles of incident and reflected light, the light's polarization, the

25 March 2026 03:03:50

© Author(s) 2025

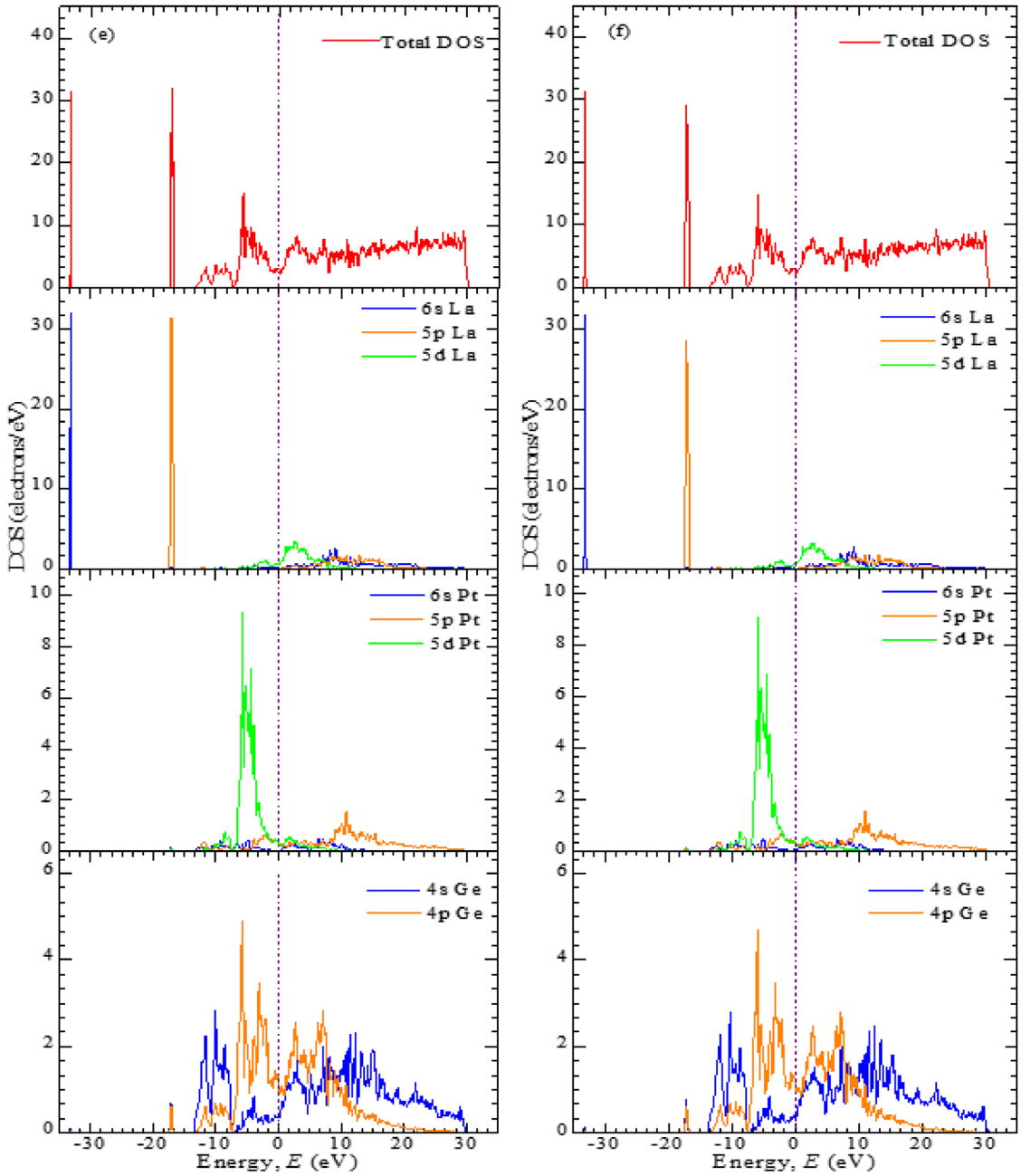

FIG. 6. Total and partial density of states (DOS) of $LaPtGe_3$ at (e) $P = 20$ GPa and (f) $P = 25$ GPa.

material type (such as metal or plastic), its chemical composition and structure, and the state of the material and its surface—factors like temperature, surface roughness, and the degree of oxidation or contamination. Figure 7(a) shows the reflectivity spectra of the $LaPtGe_3$ compound along the [100], [010], and [001] directions at different external pressures. From Fig. 7(a), it is observed that the reflectivity starts with 0.78, then it decreases with the increase of photon energy. Above 17.24 eV, a sharp increase in reflectivity is observed. At the photon energy of 21.92 eV, a sharp peak is observed in all directions where the reflectivity is about 0.27. As shown in Fig. 7(a), reflectivity

25 March 2026 03:03:50

© Author(s) 2025

TABLE III. Total and partial DOS of $LaPtGe_3$ under different pressures.

	Partial densities of states (PDOS) (electrons/eV)								
	La			Pt			Ge		
Pressure, P (GPa)	6s	5p	5d	6s	5p	5d	4s	4p	Total DOS (electrons/eV)
0	0.143	0.0405	0.510	0.028	0.221	0.320	0.386	1.169	2.554
5	0.128	0.0495	0.538	0.034	0.213	0.318	0.378	1.158	2.565
10	0.126	0.0559	0.575	0.037	0.215	0.325	0.381	1.164	2.627
15	0.140	0.0606	0.596	0.041	0.224	0.333	0.391	1.178	2.694
20	0.142	0.0635	0.619	0.040	0.236	0.338	0.395	1.192	2.748
25	0.143	0.0639	0.626	0.039	0.242	0.335	0.396	1.182	2.745

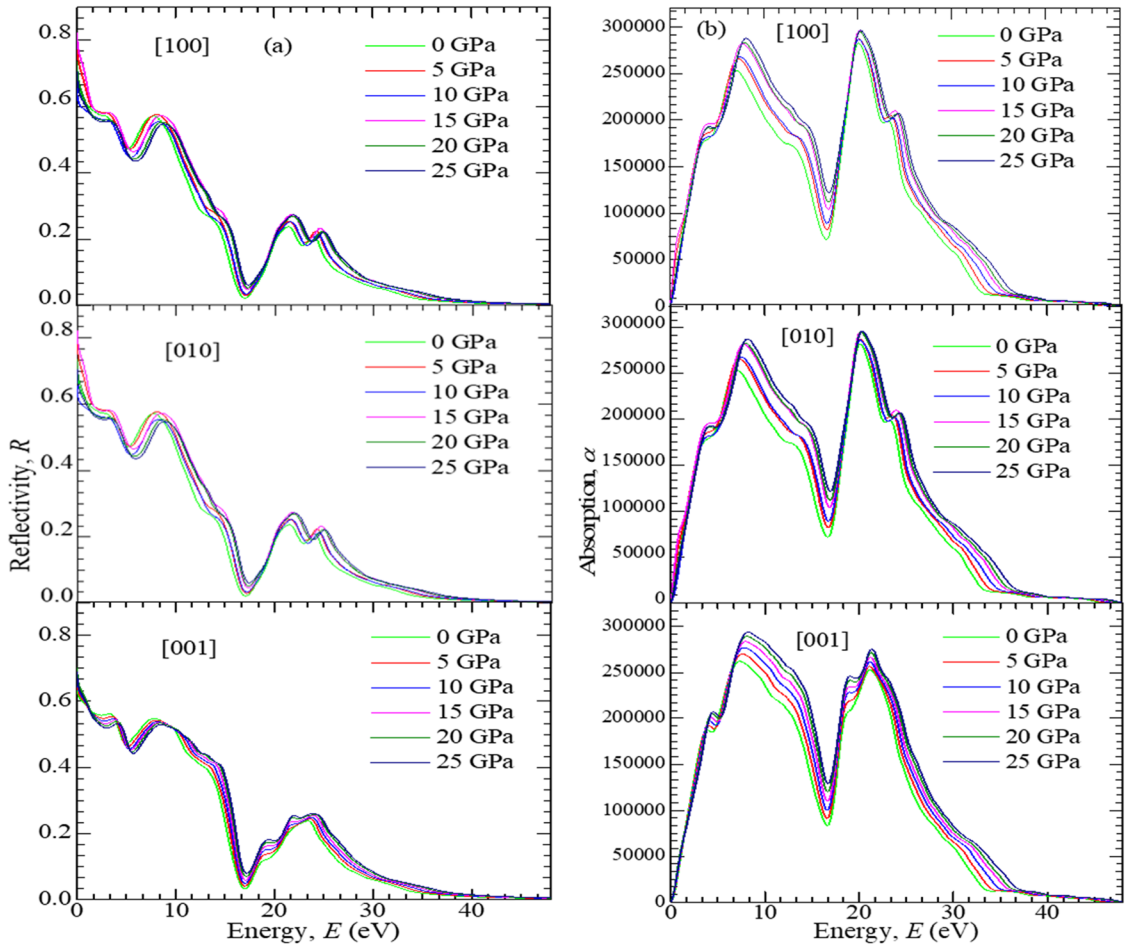

FIG. 7. Effect of pressure on (a) reflectivity and (b) absorption of $LaPtGe_3$ along the [100], [010], and [001] directions.

rises with the increase in externally applied pressure. The elevated reflectivity in the high-energy region makes it a suitable material for coatings to prevent solar heating. The reflectivity is fully dropped in the higher energy regions above 45 eV. It is also observed that the change of reflectivity with photon energy along the [100] and [010] directions is almost similar, whereas this change of reflectivity at around 17 eV is slightly different along the [001] direction due to the anisotropy along the c-axis.

25 March 2026 03:03:50

© Author(s) 2025

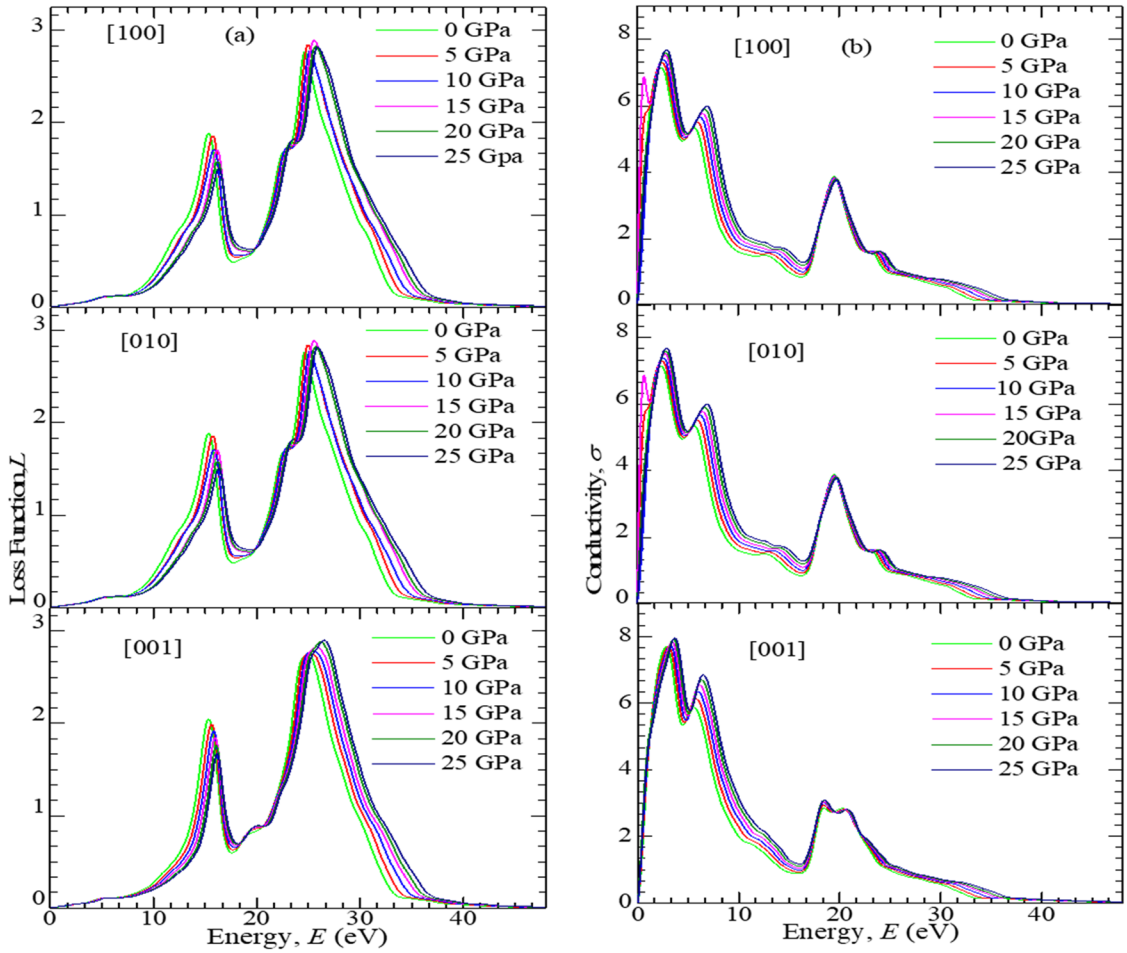

FIG. 8. (a) Loss function and (b) conductivity of $LaPtGe_3$ along [100], [010], and [001] directions at different applied pressures.

Figure 7(b) shows the absorption spectra of the $LaPtGe_3$ compound along the [100], [010], and [001] directions. The absorption coefficient defines the extent to which light of a specific wavelength can penetrate a material before being absorbed. It is influenced by both the material and the wavelength of the absorbed light. For the $LaPtGe_3$ compound, the absorption spectra begin at zero photon energy, indicating its metallic behavior. Several peaks are observed in the spectra, where the first peak is in the infrared region and the other two peaks are in the ultraviolet region. The maximum absorption is observed at around 20.50 eV, which reveals that the materials tend to become transparent after these energies. No absorption is found from the energy above 50 eV, which indicates that the compound $LaPtGe_3$ is transparent above this energy. By increasing external pressure, the absorption also increases. It indicates that the compound under large pressure is more suitable to use in a solar cell rather than under ambient pressure. The anisotropic behavior along the [001] direction is also observed in the absorption spectra in all the pressure ranges from 0 to 37 GPa.

Photoconductivity is a well-known optical and electrical phenomenon where the electrical conductivity of a material increases as a result of light absorption.[30] In this study, the calculated conductivity spectra are shown in Fig. 8(b). The effect of external pressure on the conductivity is found in all energy regions under ambient to 25 GPa pressure along all polarization directions.

It is seen that the conductivity increases with the increase of pressure. The photoconductivity appears to start at zero photon energy, as shown in Fig. 8(b), which indicates that $LaPtGe_3$ has no bandgap and shows the metallic nature. The metallic nature of $LaPtGe_3$ can also be confirmed from the band structure calculation. The photoconductivity and electrical conductivity of this material increase with photon energy,[31] with the maximum peak observed at 2.90 eV in the visible region along the [100] and [010] directions. In contrast, the maximum peak is found at around 3.5 eV along the [001] direction. Above 3.5 eV, two peaks with lower conductivity at around 6.90 and 19.63 eV are also observed in the conductivity spectra. Therefore, a large pressure is better to use this compound

25 March 2026 03:03:50

© Author(s) 2025

as a photoconductor rather than ambient pressure. The anisotropic nature along the [001] direction is visible in the conductivity spectra in all the pressure ranges from 0 to 25 GPa.

The loss function represents the energy lost by the first electron traveling through the material, with the maximum energy loss corresponding to the bulk plasma frequency, ω_P.[32] For $LaPtGe_3$, the observed bulk plasma frequency in the loss function spectra is 25.65 eV, as shown in Fig. 8(a).

When the incident photon energy exceeds the bulk plasma frequency, the material becomes transparent. An increase in external pressure also leads to an increase in the loss function. The refractive index indicates the degree to which light is bent or refracted when entering a material. Figures 9(a) and 9(b) show the real and imaginary parts of the refractive index, respectively. It is observed that the refractive index is initially high, then significantly decreases in the infrared region, and gradually decreases in the visible and ultraviolet regions. It is observed that the refractive index of $LaPtGe_3$ decreases steadily with the increase in external pressure. A noticeable anomaly in the real part of the refractive index occurs around 8.9 eV along the [001] direction, which is not present in other directions, confirming the anisotropic nature of $LaPtGe_3$ along the *c*-axis.

The dielectric function of a material characterizes its electrical and optical properties as a function of 35 frequencies. It describes the polarization and absorption behavior of the material.[33] The real part (ε_1) and imaginary part (ε_2) of the dielectric functions for $LaPtGe_3$ are shown in Figs. 10(a) and 10(b), respectively. The large negative value of ε_1 suggests the Drude-like metallic behavior of $LaPtGe_3$. The real part of ε_1 decreases to zero from below, and the imaginary part, ε_2, approaches zero from above, further confirming its metallic characteristics. As seen in Fig. 10(a), the real part of the dielectric function, ε_1, reaches zero at around 0.45 eV and then approaches nearly one in the high-energy (ultraviolet) region. The complex dielectric function ε_2, which represents the linear response of electromagnetic radiation, typically describes the material's optical properties. Figure 10(b) shows that the imaginary part of the dielectric function tends to zero in the high-energy region.

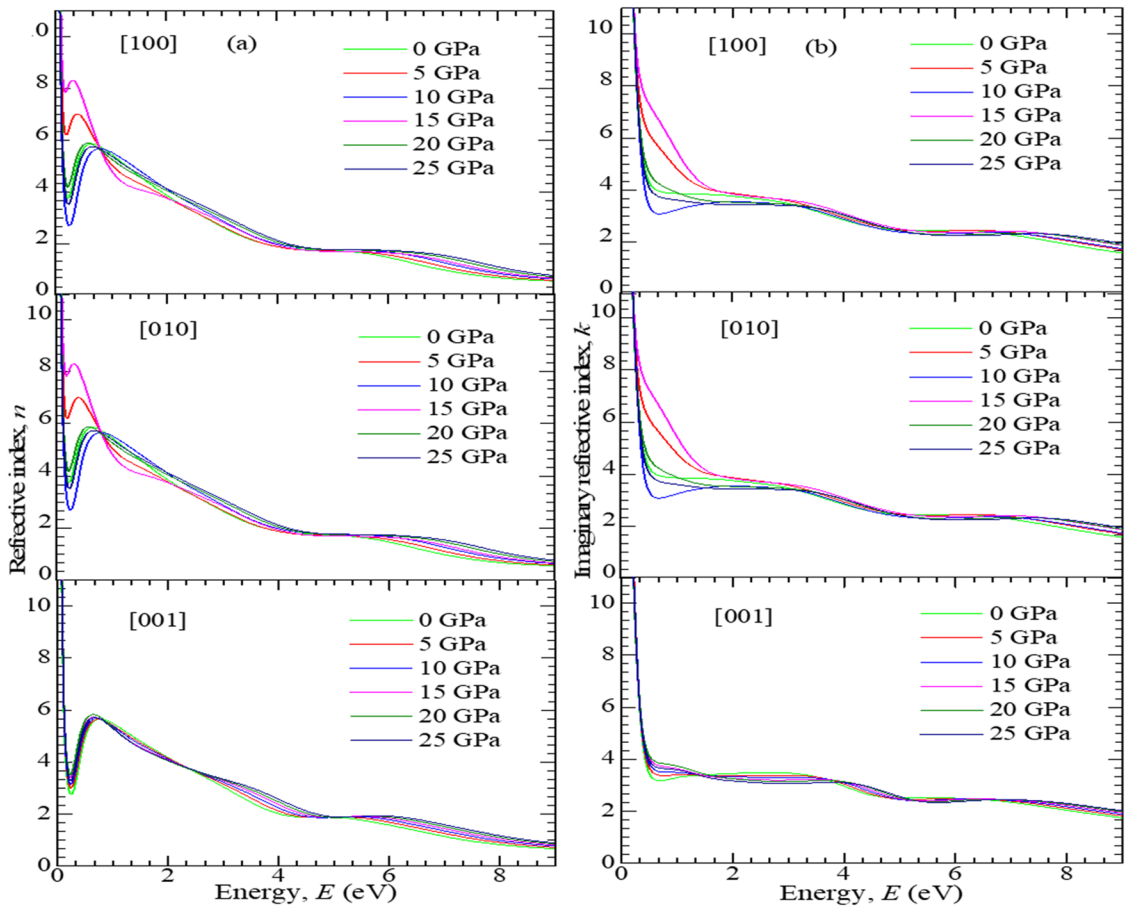

FIG. 9. (a) Real and (b) imaginary part of the reflective index of $LaPtGe_3$ along the [100], [010], and [001] directions at different pressures.

25 March 2026 03:03:50

© Author(s) 2025

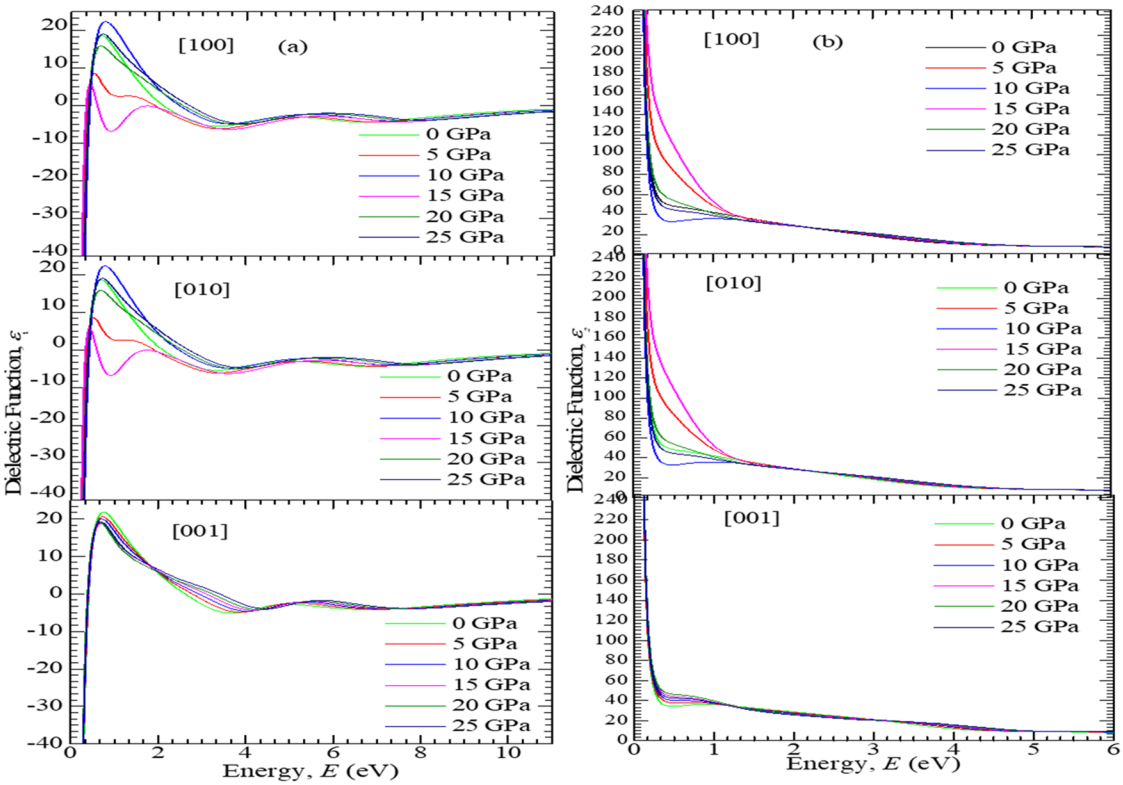

FIG. 10. (a) Real part and (b) imaginary part of dielectric functions of $LaPtGe_3$ along [100], [010], and [001] directions at different pressures.

IV. CONCLUSION

In conclusion, the electronic and optical properties of tetragonal $LaPtGe_3$ were investigated using density functional theory. Band structure calculations revealed that some bands overlap with the Fermi level, ranging from approximately −3–1 eV, which indicates the material's metallic nature. The density of states (DOS) calculations show a significant contribution from the Ge-4*p* states at the Fermi level, suggesting that these states are responsible for the electrical conductivity, reinforcing the metallic behavior of $LaPtGe_3$. The total DOS at the Fermi level slightly decreases as external pressure increases, indicating a reduction in the material's electrical conductivity and metallic character. This decrease may be linked to the shortening of the Ge–Ge bond length under pressure. These changes in the DOS and bond length could affect other properties of $LaPtGe_3$, such as its optical and thermodynamic characteristics. Reflectivity increases with applied external pressure, and the variation in reflectivity with photon energy along the [100] and [010] directions is nearly identical, except around 17 eV along the [001] direction, where anisotropy along the *c*-axis is observed. The observed absorption spectra start from zero photon energy, which indicates the metallic behavior of $LaPtGe_3$. Maximum absorption is observed at around 20.50 eV. No absorption is found from the energy above 50 eV, which indicates that the compound $LaPtGe_3$ becomes completely transparent above this energy. As external pressure increases, the absorption of $LaPtGe_3$ also increases, suggesting that the compound is more suitable for use in solar cells under high pressure compared to ambient pressure. Anisotropic behavior along the [001] direction is observed in the absorption spectra across all pressure ranges from 0 to 25 GPa. Photoconductivity is seen at zero photon energy, indicating that $LaPtGe_3$ has no bandgap, which further confirms its metallic nature. This anisotropic behavior is also evident in the conductivity spectra across the same pressure ranges. The bulk plasma frequency observed in the loss function spectra is 25.65 eV for $LaPtGe_3$, and this value can be increased by applying external pressure. The refractive index starts high and then sharply decreases in the infrared region, gradually reducing in the visible and ultraviolet regions. With increasing external pressure, the refractive index of $LaPtGe_3$ decreases progressively. The real part of the dielectric function, ε_1, reaches zero from below, and the imaginary part, ε_2, approaches zero from above, both confirming the metallic characteristics of $LaPtGe_3$.

AUTHOR DECLARATIONS

Conflict of Interest

The authors have no conflicts to disclose.

25 March 2026 03:03:50

© Author(s) 2025

Author Contributions

Md. Karimul Islam: Investigation (equal); Methodology (equal); Software (equal); Writing – original draft (equal). **Nilufer Yesmin Tanisa**: Methodology (equal); Supervision (equal); Writing – review & editing (equal). **Mosfiqur Rahman**: Supervision (equal); Writing – review & editing (equal). **Abul Monsur Musa**: Visualization (equal); Writing – review & editing (equal). **Tareque Aziz**: Visualization (equal); Writing – review & editing (equal). **Md. Moiful Alam**: Writing – review & editing (equal). **Asif Pervez**: Writing – review & editing (equal).

DATA AVAILABILITY

Data sharing is not applicable to this article as no new data were created or analyzed in this study.

REFERENCES

[1] A. Weiland, K. Wei, G. T. McCandless, J. B. Felder, L. J. Eddy, R. E. Baumbach, and J. Y. Chan, "Strongly correlated electron behavior in a new member of the $A_{n+1}B_nX_{3n+1}$ homologous series: $Ce_7Co_6Ge_{19}$," Phys. Rev. Mater. **4**(7), 074408 (2020).

[2] C. Zheng and R. Hoffmann, "Complementary local and extended views of bonding in the $ThCr_2Si_2$ and $CaAl_2Si_2$ structures," J. Solid State Chem. **72**(1), 58–71 (1988).

[3] K. Singh, S. S. Ashutosh, and S. C. Peter, "Diversity in crystal structure and physical properties of $RETX_3$ (*RE*–rare earth, *T*–transition metal, *X*–main group element) intermetallics," Chem. Rec. **22**(5), e202100317 (2022).

[4] U. Häussermann, S. Amerioun, L. Eriksson, C.-S. Lee, and G. J. Miller, "The s–p bonded representatives of the prominent $BaAl_4$ structure type: A case study on structural stability of polar intermetallic network structures," J. Am. Chem. Soc. **124**(16), 4371–4383 (2002).

[5] *Handbook on the Physics and Chemistry of Rare Earths*, edited by L. Eyring, K. A. Gschneidner, and G. H. Lander (Elsevier, 2002), Vol. 32.

[6] G. R. Stewart, "Non-Fermi-liquid behavior in *d*- and *f*-electron metals," Rev. Mod. Phys. **73**(4), 797 (2001).

[7] C. Cao, R. Klingeler, N. Leps, G. Behr, and W. Löser, "Single crystal growth of the $ErPd_2Si_2$ intermetallic compound," J. Cryst. Growth **401**, 601–604 (2014).

[8] H. Fujii and A. Sato, "Crystal structure of ternary germanides SrM_2Ge_2 (M = Ni and Ir)," J. Alloys Compd. **487**(1–2), 198–201 (2009).

[9] S. Baran, M. Bałanda, A. Hoser, K. Nenkov, B. Penc, and A. Szytuła, "Nature of magnetic phase transitions in $TbCu_2X_2$ (X = Si, Ge) and $HoCu_2Si_2$ compounds," J. Alloys Compd. **507**(1), 16–20 (2010).

[10] G. A. Cabrera-Pasca, A. W. Carbonari, R. N. Saxena, B. Bosch-Santos, J. A. H. Coaquira, and J. Filho, "Magnetic hyperfine field at highly diluted Ce impurities in the antiferromagnetic compound $GdRh_2Si_2$ studied by perturbed gamma–gamma angular correlation spectroscopy," J. Alloys Compd. **515**, 44–48 (2012).

[11] E. Mörsen, B. D. Mosel, W. Müller-Warmuth, M. Reehuis, and W. Jeitschko, "Mössbauer and magnetic susceptibility investigations of strontium, lanthanum and europium transition metal phosphides with $ThCr_2Si_2$ type structure," J. Phys. Chem. Solids **49**(7), 785–795 (1988).

[12] I. R. Shein and A. L. Ivanovskii, "Structural and electronic properties of the 17 K superconductor $Sr_2ScFePO_3$ in comparison to $Sr_2ScFeAsO_3$ from first principles calculations," Phys. Rev. B **79**(24), 245115 (2009).

[13] F. Ronning, N. Kurita, E. D. Bauer, B. L. Scott, T. Park, T. Klimczuk, R. Movshovich, and J. D. Thompson, "The first order phase transition and superconductivity in $BaNi_2As_2$ single crystals," J. Phys.: Condens. Matter **20**(34), 342203 (2008).

[14] E. D. Bauer, F. Ronning, B. L. Scott, and J. D. Thompson, "Superconductivity in $SrNi_2As_2$ single crystals," Phys. Rev. B **78**(17), 172504 (2008).

[15] M. A. Khan, *Non-Centrosymmetric Superconductivity and Magnetism in the Presence of Broken Symmetries* (Louisiana State University and Agricultural and Mechanical College, 2017).

[16] D. Stasko, "Pressure effects on physical properties of a selected Ce-based compound," M.S. thesis (Charles University, 2020).

[17] M. Feig, M. Nicklas, M. Bobnar, W. Schnelle, U. Schwarz, A. Leithe-Jasper, C. Hennig, and R. Gumeniuk, "Superconductivity and magnetism in noncentrosymmetric $LaPtGe_3$ and $CePtGe_3$," Phys. Rev. B **98**(18), 184516 (2018).

[18] J. Song, Y. Qin, D. Shi, X. Chen, W. Li, R. Ren, Y. Wang, X. Yang, and C. Cao, "A high-throughput screening and discovery of lanthanum based ternary noncentrosymmetric superconductors with ZrNiAl-structure from ab initio calculations," J. Phys. Chem. Solids **184**, 111676 (2024).

[19] N. Kumar, P. K. Das, R. Kulkarni, A. Thamizhavel, S. K. Dhar, and P. Bonville, "Antiferromagnetic ordering in $EuPtGe_3$," J. Phys.: Condens. Matter **24**(3), 036005 (2011).

[20] H. Y. Uzunok, T. Zafer, H. M. Tütüncü, E. Karaca, S. Bağcı, and G. P. Srivastava, "Probing physical properties and superconductivity of noncentrosymmetric superconductors LaPtGe and $LaPtGe_3$: A first-principles study," Comput. Mater. Sci. **185**, 109949 (2020).

[21] M. Usman Ghani, M. Sagir, M. Bilal Tahir, H. I. Elsaeedy, S. Nazir, H. Alrobei, and M. Alzaid, "CASTEP investigation of structural, electronic, and optical properties of halide perovskites $RbXCl_3$ (X = Ge, Sn, Pb) for solar cell applications," Inorg. Chem. Commun. **155**, 111007 (2023).

[22] M. Ernzerhof and G. E. Scuseria, "Assessment of the Perdew–Burke–Ernzerhof exchange-correlation functional," J. Chem. Phys. **110**(11), 5029–5036 (1999).

[23] P.. Schwerdtfeger, "The pseudopotential approximation in electronic structure theory," ChemPhysChem **12**(17), 3143–3155 (2011).

[24] J.-H. Lee, T. Shishidou, and A. J. Freeman, "Improved triangle method for two-dimensional Brillouin zone integrations to determine physical properties," Phys. Rev. B **66**(23), 233102 (2002).

[25] W.. Zhao, "A Broyden–Fletcher–Goldfarb–Shanno algorithm for reliability-based design optimization," Appl. Math. Modell. **92**, 447–465 (2021).

[26] R. Diale, B. N. Duduzile Nkomo, and P. Maje, "The use of DFT-based *ab initio* technique to determine the stability difference in B_2 Ti-PGM compounds," in *Density Functional Theory-New Perspectives and Applications* (IntechOpen, 2023).

[27] A. S. Hassanien, "Studies on dielectric properties, opto-electrical parameters and electronic polarizability of thermally evaporated amorphous $Cd_{50}S_{50-x}Se_x$ thin films," J. Alloys Compd. **671**, 566–578 (2016).

[28] A. S. Hassanien and I. Sharma, "Optical properties of quaternary a-$Ge_{15-x}Sb_xSe_{50}Te_{35}$ thermally evaporated thin-films: Refractive index dispersion and single oscillator parameters," Optik **200**, 163415 (2020).

[29] Y. Yanase and M. Sigrist, "Superconductivity and magnetism in non-centrosymmetric system: Application to $CePt_3Si$," J. Phys. Soc. Japan **77**(12), 124711–124711 (2008).

[30] N. V. Joshi, *Photoconductivity: Art: Science and Technology* (Routledge, 2017).

[31] M. Freitag, Y. Martin, J. A. Misewich, R. Martel, and Ph. Avouris, "Photoconductivity of single carbon nanotubes," Nano Lett. **3**(8), 1067–1071 (2003).

[32] C. H. Chen, J. Silcox, and R. Vincent, "Electron-energy losses in silicon: Bulk and surface plasmons and Čerenkov radiation," Phys. Rev. B **12**(1), 64 (1975).

[33] J. Mistrik, S. Kasap, H. E. Ruda, C. Koughia, and J. Singh, "Optical properties of electronic materials: Fundamentals and characterization," in *Springer Handbook of Electronic and Photonic Materials* (Springer, 2017), p. 1.

25 March 2026 03:03:50

© Author(s) 2025